Transp Porous Med (2012) 93:815–829
DOI 10.1007/s11242-012-9985-0

The Effective Permeability of Cracks and Interfaces in Porous Media

Franck J. Vernerey

Received: 7 October 2011 / Accepted: 7 March 2012 / Published online: 22 March 2012

Abstract The presence of interfaces in fluid/solid biphasic media is known to strongly

However, as any continuum theories, mixture formulations are not readily appropriate for describing discontinuous fields originating from the presence of interfaces (such as cracks or embedded membranes) within a material's microstructures. This represents a challenge since such discontinuities may critically affect the nature of the interstitial fluid flow as well as the elastic deformations. Various strategies have therefore been elaborated to address this issue, with a particular interest on describing fluid flow in a fractured porous media (Barthelemym 2009; Liolios and Exadaktylos 2008; Pouya and Ghabezloo 2008; Ghabezloo and Pouya 2008). In the case where interfaces are cracks, fluid flow has traditionally been described by a Poiseuille-type distribution that can be determined by carefully handling boundary conditions between the free fluid flow in the interface and that in the surrounding porous medium (Chandesris and Jamet 2006; Goyeaua et al. 2003). These methods particularly enabled the derivation of useful relationships between effective permeability and internal crack structure. With the same objective in mind, different approaches have later been introduced. For instance, one approach consisted in describing cracks as thin ellipsoidal inclusions for which an effective permeability could be derived using self-consistent homogenization techniques (Dormieux and Kondo 2007; Barthelemym 2009). Similarly, Lolios and Exadaktylos (2008) and later Pouya and Ghabezloo (2008), described cracks as lines of pressure discontinuity that could subsequently be used to determine the interfacial fluid flow. We note that while the above studies were extremely useful in estimating the effective permeability of microcracked porous media, they did not consider the case of a porous material interfaces nor did they consider the coupling between solid deformation and interface flow.

To tackle these shortcomings, we have recently introduced a general theory (Vernerey 2011) that can describe the combined deformation and fluid flow in an elastic porous medium with interfaces. Due to its flexibility, the formulation is able to characterize a variety of phenomena including both interface deformation (Gurtin et al. 1998), surface tension (Farsad et al. 2010; Vernerey and Farsad 2011b) as well as interface fluid flow and its coupling with elastic deformations. However, as it is based on macroscopic assumptions, the theory does not specify the links between constitutive relation and the nature of the underlying structure of the medium which, as a consequence, precludes any applications to real materials and interfaces. This article addresses this issue by presenting an analytical analysis of fluid flow in a porous interface in order to provide a clear link between macroscopic interface permeabilities and the microscopic nature of the interface it represents (including the thickness, permeability, effective viscosity of the interface, as well as those of its surrounding medium). To reconcile macroscopic and microscopic interface descriptions, we first determine an expression for interface flows when macroscopic pressure gradients are present by solving the Darcy–Brinkman equation in the interface neighborhood. Upon obtaining the solution, the concept of thickness averaging introduced in our earlier work (Vernerey 2011) is invoked in order to compute effective interface permeabilities in terms of interface and bulk properties. Besides obtaining useful relationships relating macro- and microscopic interface descriptions, the present analysis provides an interesting insight, both qualitatively and quantitatively, onto the nature of fluid flow in interfaces whose properties may drastically differ from that of the surrounding medium.

This article is organized as follows. In the next section, we provide a short summary of the theoretical framework used to model fluid flow in porous media with thin interfaces. In Sect. 3, we concentrate on the microscopic view of the interface and derive expressions for the normal and tangential flow across an interface of finite thickness, when subjected to macroscopic pressure gradients. The results are then used in Sect. 4 to determine key

Table 1 Nomenclature

Definition	Symbol	Unit
Average of macroscopic fields across interface	{}	n/a
Jump in macroscopic fields across interface	[ ]	n/a
component of continuum fields normal to interface	Superscript $\perp$	n/a

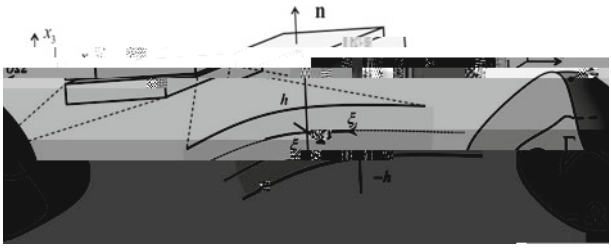

Fig. 1 Porous solid containing interfaces and the normal vector to interfaces

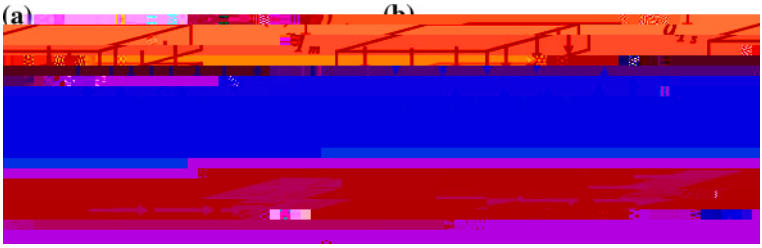

Fig. 2 Illustration of normal and tangential fluid velocities in the interface

where φ is a scalar quantity describing the bulk porosity. Moreover, considering an interface with constant porosity $\bar{\varphi}$, mass conservation in was shown to take the following form for an incompressible fluid:

$$\mathrm{div}^{\parallel}\left(\bar{\varphi}\mathbf{q}_{\xi}^{\parallel}\right) + \frac{[\varphi\mathbf{q}\cdot\mathbf{n}]}{2} = 0 \tag{6}$$

$$\mathrm{div}^{\parallel}\left(\bar{\varphi}\mathbf{q}^{\parallel}\right) + \frac{1}{2}\left(\{\varphi\mathbf{q}\cdot\mathbf{n}\} - \bar{\varphi}\ {}^{\perp}_{\xi}\right) = 0, \tag{7}$$

where $\mathbf{q}_{\xi}^{\parallel} = {}^{\parallel}_{\xi}\mathbf{t}$ and $\mathbf{q}^{\parallel} = {}^{\parallel}\mathbf{t}$ are the tangential interface velocity vectors whose direction is given by the unit tangential vector $\mathbf{t}$ to the interface. Moreover, the symbol $\mathrm{div}^{\parallel}$ denotes the surface divergence operator, and is a moment of inertia-like quantity defined as:

$$= \frac{1}{(2\ )^3}\int_{-}\xi^2 \mathrm{d}\xi\ = \frac{1}{12}. \tag{8}$$

Equation (6) describes how tangential velocities are affected by the amount of fluid coming from the bulk into the interface (or vice versa). Similarly, Eq. (7) represents the mass balance in terms of $\mathbf{q}^{\parallel}$ and the average normal velocity $\mathbf{q}\cdot\mathbf{n}$ passing though the interface. The above equations therefore naturally describe the coupling between fluid flow in the bulk and interface.

2.3 Constitutive assumptions

Traditionally, the steady flow of a fluid through a porous medium has been described by Darcy's law in the form shown in (1). However, when interfaces are present, significant fluid velocity gradients may develop in the vicinity of the interface, giving rise to boundary layers. The characteristic length-scale of the boundary layers is very sensitive to the fluid viscosity, a phenomenon that is well captured by the Darcy–Brinkman equation:

$$\mathbf{q} = \frac{\kappa^{\mathrm{B}}}{\mu}\left(-\nabla\ + \mu_{\mathrm{e}}^{\mathrm{B}}\nabla^2\mathbf{q}\right), \tag{9}$$

where $\mu_{\mathrm{e}}^{\mathrm{B}}$ is the effective Brinkman viscosity, and κ^{B} is the isotropic permeability of the medium. The first term within the parenthesis may be interpreted as a driving force arising from a pressure gradient and the second term represents a resisting force due to fluid viscosity. Now turning to interface flows, we have shown in Vernerey (2011) that for the case of isotropic interfaces, a Darcy-type relation can be established in terms of four macroscopic scalar permeabilities $\kappa_{\xi}^{\perp}$, $\kappa_{\xi}^{\parallel}$, $\kappa^{\perp}$, and $\kappa^{\parallel}$ such that:

$$\overset{\perp}{\varsigma} = -\frac{\kappa_{\varsigma}^{\perp}}{\mu}\frac{[\ ]}{2} \qquad \overset{\parallel}{\varsigma} = -\frac{\kappa_{\varsigma}^{\parallel}}{\mu}\{\nabla\ \}^{\parallel} \tag{10}$$

$$^{\perp} = -\frac{\kappa^{\perp}}{\mu}[\nabla\ ]^{\perp} \qquad ^{\parallel} = -\frac{\kappa^{\parallel}}{\mu}[\nabla\ ]^{\parallel}. \tag{11}$$

We note here that the above permeabilities physically represent the resistance of the interface to flow; More specifically, the permeabilities $\kappa_{\varsigma}^{\perp}$ and $\kappa_{\varsigma}^{\parallel}$ provide a measure of the resistance

$$\{\kappa, \mu_e\} = \left\{\kappa \ , \mu_e\right\} \quad \xi \in [- \ , \ ] \tag{13}$$

$$= \left\{\kappa^B, \mu_e^B\right\} \quad \xi \in]-\infty, - \ [\cup] \ , \infty[. \tag{14}$$

In addition, the pressure gradient profile in the interface may be written as a Taylor series around the center of the interface ($\xi = 0$) in terms of the macroscopic mean pressure gradient $\{\nabla \ \}$ and the macroscopic jump in pressure gradient $[\nabla \ ]$ across as:

$$\begin{aligned} \nabla \ (\xi \ ) &= \{\nabla \ \} - \frac{[\nabla \ ]}{2} \quad \xi \in]-\infty, - \ [\\ &= \{\nabla \ \} + \frac{[\nabla \ ]}{2}\xi \ + \mathcal{O}\left(\xi^2\right) \quad \xi \in [- \ , \ ] \\ &= \{\nabla \ \} + \frac{[\nabla \ ]}{2} \quad \xi \in] \ , \infty[\end{aligned} \tag{15}$$

Upon solving the microscopic flow $\tilde{\mathbf{q}}$ with (12), the macroscopic velocities $\mathbf{q}_{\kappa}$ and $\mathbf{q}$ are found by the averaging operation:

$$\mathbf{q}_{\kappa} = \frac{1}{2}\int_{-}\tilde{\mathbf{q}}(\xi \ )\mathrm{d}\xi \ , \quad \mathbf{q} \ = \frac{1}{(2 \ )^2}\int_{-}\tilde{\mathbf{q}}(\xi \ )\xi \ \mathrm{d}\xi \ . \tag{16}$$

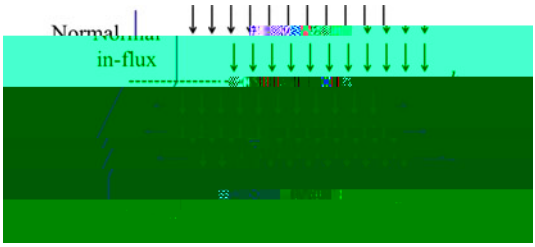

Fig. 4 Schematic displaying the change of normal flow through the interface. Note that for incompressible fluids, a variation of flow is only possible if tangential flow is allowed

where we used the fact that $\{\nabla\ \}^{\perp} = [\ ]/2\ $. Substituting (19) into (18) immediately leads to an expression for the normal interface velocity $\tilde{\ }$:

$$\tilde{\ } = -\frac{\kappa}{2\mu}\left([\ ] + [\nabla\ ]^{\perp}\xi\right). \tag{20}$$

This expression shows that the normal velocity arises from a jump in pressure across the interface and exhibits a linear variation when a jump $[\nabla\ ]^{\perp}$ in pressure gradient is present. Note that in order to ensure that the condition of incompressibility at the microscale, one should verify that $\mathrm{div}\tilde{\mathbf{q}} = \partial\tilde{\ }/\partial\xi\ + \partial\tilde{\ }/\partial\xi\ = 0$. Assessing the divergence with the help of Eq. (20) implies that the normal flow generates a tangential flow $\tilde{\ }$ that varies in the tangential direction such that $\partial\tilde{\ }/\partial\xi\ = -\frac{\kappa}{2}$

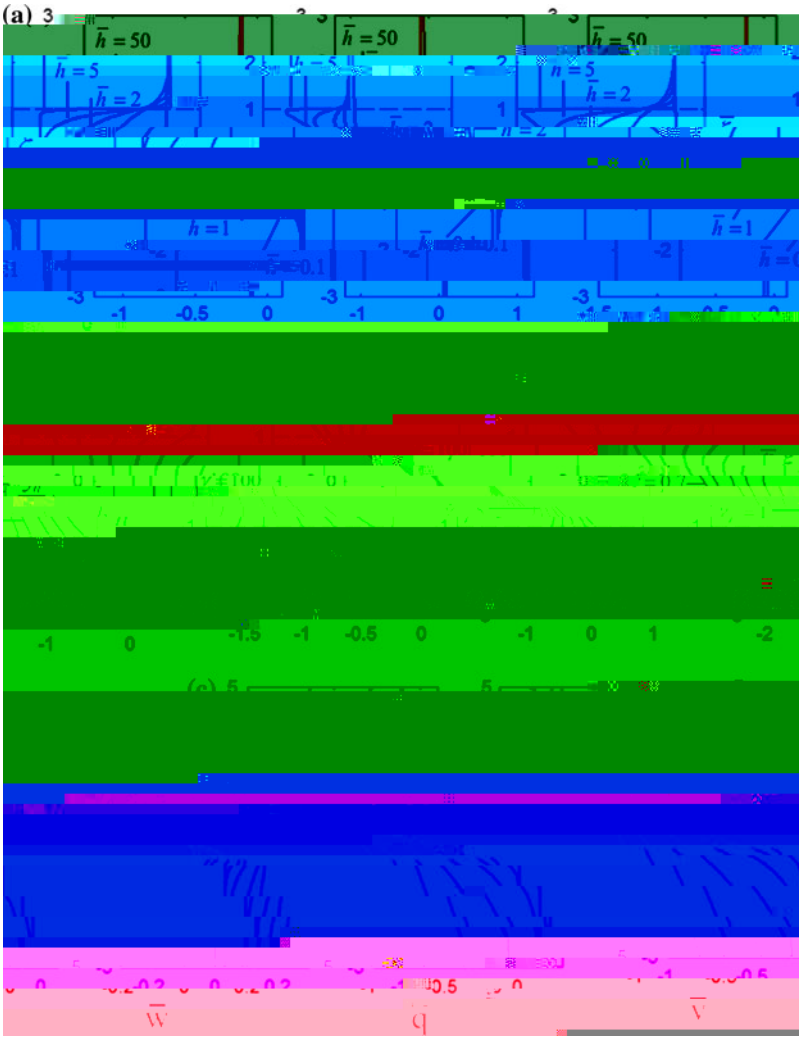

Fig. 5 **a** Effect of interface thickness on tangential flow at $\gamma = 10$ and $\beta = 1$. **b** Effect of interface permeability on tangential flow at $\bar{\ } = 1$ and $\beta = 1$. **c** Effect of effective viscosity on tangential flow at $\bar{\ } = 1$ and $\gamma = 10$

The final solution $\tilde{\ }$ is subsequently written as a combination of $\bar{v}$ and $\bar{w}$ as:

$$\tilde{\ } = \frac{\kappa}{\mu}\left(\bar{v}\{\nabla \ \}^{\parallel} + \bar{w}\frac{[\nabla \ ]^{\parallel}}{2}\right). \tag{35}$$

It can be seen that the nature of the interface tangential flow mainly depends on three parameters that consists of $\bar{\ }$, β and γ as depicted in Fig. 5. It is first important to note that interface thickness is defined in relation to the length-scale defined by $\sqrt{\kappa \ \mu_e/\mu}$. In other words, a given value of may be considered small for a highly viscous fluid and a small interface permeability, while it may be considered large in the opposite situation. Figure 5a shows the nondimensional tangential velocities for different values of $\bar{\ }$ when $\gamma = 10$ and $\beta = 1$. Generally, the figure shows that for small values of $\bar{\ }$, the interface dimensions are

too small in order for the tangential flow to fully develop independently from the bulk flow. However, as $\bar{}$ increases to values close to unity, interface flow starts developing but is still constrained by a transition zone between bulk and interface. However, as $\bar{}$ increases to larger values, the characteristic length of the transition dramatically reduces such that interface and bulk flows become quasi independent at $\bar{} = 50$. These observations are valid for both the symmetric and antisymmetric parts of the flows, which implies that the development of both the mean and first moment of interface flow are promoted by large values of $\bar{}$.

The effect of interface permeability, characterized by the ratio $\gamma = \kappa \ /\kappa^{\mathrm{B}}$ is also illustrated in Fig. 5b for constant interface thickness ($\bar{} = 1$) and effective viscosity ratio ($\beta = 1$). As expected, interface flow is slower in the interface for $\gamma < 1$ and faster for $\gamma > 1$. In addition, as γ increases, the first moment of interface flow can fully develop in the interface, which triggers a sharp flow discontinuity across the interface. However, as γ decreases below unity, the interface becomes more resistant to , and the transition region (or boundary layer) mostly occurs in the bulk.

Similarly, the effective viscosity ratio $\beta = \mu_{\mathrm{e}}/\mu_{\mathrm{e}}^{\mathrm{B}}$ plays a large influence on the extend of the boundary layer near the interface as shown in Fig. 5c. Generally, the extent of the influence of interface flow on bulk flow increases with decreasing β (or increasing bulk viscosity $\mu_{\mathrm{e}}^{\mathrm{B}}$).

4 Macroscopic Permeabilities and Their Relation to Microscopic Interface Properties

To bridge micro and macroscopic interface descriptions, we now seek to express macroscopic permeabilities introduced in (10) and (11) in terms of interface properties $\bar{}$, γ, and β. This may be accomplished by projecting the averaging operation defined in (16) along the normal

4.2 Tangential permeabilities

In turn, macroscopic tangential permeabilities are obtained by projecting (16) onto the tangential direction as follows:

$$\ddot{\kappa}^{\parallel} = \frac{1}{2}\ddot{\kappa}$$

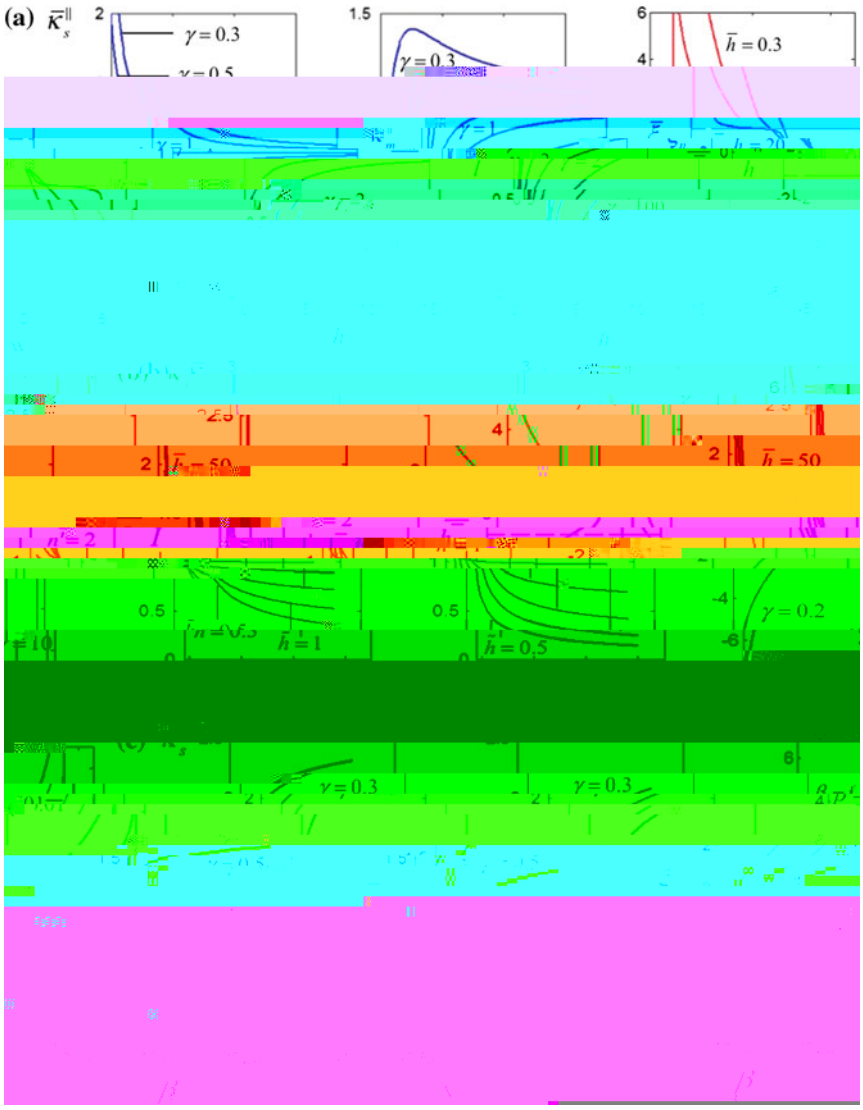

Fig. 6 **a** Effect of interface thickness effective permeabilities $\bar{\kappa}_s^{\parallel}$ and $\bar{\kappa}^{\parallel}$. For all cases, $\beta = 1$. Note that the permeability $\bar{\kappa}^{\parallel}$ exhibits a maximum around $\bar{} = 1$ when $\gamma < 1$. This can be explained in terms of velocity ratios as shown in the last figure for $\gamma = 0.2$ and $\beta = 1$. It can clearly be seen that the maximum flow $\parallel$ is observed when $\bar{} = 1$. **b** Effect of permeability ratio γ

for large thickness ($\bar{} \to \infty$), the curves converges to horizontal lines corresponding to $\kappa_{\varsigma}^{\parallel} = \kappa$ and $\kappa^{\parallel} = \kappa$.

Finally, Fig. 6c illustrates the role of permeability ratio $\beta = \mu_{\mathrm{e}}/\mu_{\mathrm{e}}^{\mathrm{B}}$ on bulk/interface interactions. Generally, as β increases, the effect of bulk velocity on interface permeabilities becomes more and more pronounced. This generally tends to increase $\kappa_{\parallel}$ when $\gamma < 1$ (i.e., when bulk velocity is larger than interface velocity) and decrease $\kappa_{\parallel}$ when $\gamma >$

Dormieux, L., Kondo, D.: Approche micromecanique du couplage permeabilite-endommagement. Comptes Rendus Mecanique **332**, 135–140 (2007)
Farsad, M., Vernerey, F.J., Park, H.: An extended finite element/level set method to study surface effects on the mechanical behavior and properties of nanomaterials. Int. J. Numer. Methods Eng. **84**, 1466–1489 (2010)
Ghabezloo, S., Pouya, A.: Numerical upscaling of the permeability of a randomly cracked porous medium. In: The 12th International Conference of International Association for Computer Methods and Advances in Geomechanics (IACMAG) (2008)
Goyeaua, B., Lhuillierb, D., Gobina, G., Velardec, M.: Momentum transport at a fluid–porous interface. Int. J. Heat Mass Transf. **46**(21), 4071–4081 (2003)
Gurtin, M.E., Weissmuller, J., Larche, F.: A general theory of curved deformable interfaces in solids at equilibrium. Philos. Mag. A **78**, 1093–1109 (1998)
Liolios, P.A., Exadaktylos, G.E.: A solution of steady-state fluid flow in multiply fractured isotropic porous media. Int. J. Solids Struct. **43**, 3960–3982 (2008)
Pouya, A., Ghabezloo, S.: Flow-stress coupled permeability tensor for fractured rock masses. Transp. Porous Media **32**, 1289–1309 (2008)
Sun, D.N., Gu, W.Y., Guo, X.E., Lai, W.M., Mow, V.C.: A mixed finite element formulation of triphasic mechano-electromechanical theory for charged, hydrated biological soft tissues. Int. J. Numer. Methods Eng. **45**, 1375–1402 (1999)
Truesdell, C.: Rational Thermodynamics. McGraw-Hill Series in Modern Applied Mathematics. McGraw-Hill, New York (1969)
Vernerey, F.J.: On the mechanics of interfaces in deformable porous media. Int. J. Solids Struct. doi:10.1016/j.ijsolstr.2011.07.005 (2011)
Vernerey, F.J., Farsad, M.: A constrained mixture approach to mechano-sensing and force generation in contractile cells. J. Mech. Behav. Biomed. Mater. doi:10.1016/j.jmbbm.2011.05.022 (2011a)
Vernerey, F.J., Farsad, M.: An eulerian/xfem formulation for the large deformation of cortical cell membrane. Comput. Methods Biomech. Biomed. Eng. **14**, 433–445 (2011b)
Vernerey, F.J., Foucard, L., Farsad, M.: Bridging the scales to explore cellular adaptation and remodeling. Bionanoscience. doi:10.1007/s12668-011-0013-6 (2011a)
Vernerey, F.J., Greenwald, E., Bryant, S.J.: Triphasic mixture model of cell-mediated enzymatic degradation of hydrogels. Comput. Methods Biomech. Biomed. Eng. doi:10.1080/10255842.2011.585973 (2011b)